Hodak, J. H., Henglein, A. & Hartland, G. V. Size dependent properties of Au particles: Coherent excitation and dephasing of acoustic vibrational modes. J. Chem. Phys. 111, 8613–86…

ARTICLE *in* THE JOURNAL OF CHEMICAL PHYSICS · NOVEMBER 1999

Impact Factor: 2.95 · DOI: 10.1063/1.480202

FEATURE ARTICLE

Photophysics of Nanometer Sized Metal Particles: Electron−Phonon Coupling and Coherent Excitation of Breathing Vibrational Modes

Jose H. Hodak,[†] Arnim Henglein,[‡] and Gregory V. Hartland*,[†]

Department of Chemistry and Biochemistry, and Notre Dame Radiation Laboratory, University of Notre Dame, Notre Dame, Indiana 46556-5670

Received: June 21, 2000; In Final Form: August 17, 2000

The wide variety of applications of metal nanoparticles has motivated many studies of their properties. Some important practical issues are how the size, composition and structure of these materials affect their catalytic and optical properties. In this article we review our recent work on the photophysics of metal nanoparticles. The systems that have been investigated include Au particles with sizes ranging from 2 nm diameter (several hundred atoms) to 120 nm diameter, and bimetallic core−shell particles composed of Au, Ag, Pt and/or Pb. These particles, which have a rather narrow size distribution, are prepared by radiolytic techniques. By performing time-resolved laser measurements we have been able to investigate the coupling between the electrons and phonons in the particles, and their low frequency "breathing" modes. These experiments show that for Au the time scale for electron−phonon coupling does not depend on size, in contrast to metals such as Ga and Ag. On the other hand, the frequency of the acoustic breathing modes strongly depends on the size of the particles, as well as their composition. These modes are impulsively excited by the rapid lattice heating that accompanies ultrafast laser excitation. The subsequent coherent nuclear motion modulates the transmitted probe laser intensity, giving a "beat" signal in our experiments. Unlike quantum-beats in molecules or semiconductors, this signal can be completely understood by classical mechanics.

Introduction

Nanoparticles of metals and semiconductors display many unique properties, such as size-dependent melting points and structural phase transitions,[1−3] quantum confinement of electronic states,[4−6] Coulomb blockade effects,[7−10] and size-dependent catalytic properties.[11] Over the past several years a major focus of our research has been to explore the fundamental photophysics of metal particles using ultrafast laser spectroscopy. The original goal of these experiments was to characterize the time scales for electron−electron (e−e) and electron−phonon (e−ph) scattering, and to determine whether these processes depend on factors such as the size of the particles or their composition. These are significant questions that are still not generally resolved,[12−21] and one of the objects of this review is to communicate our current understanding of e−ph coupling in metal particles. However, in the course of these experiments we also observed an unusual coherent response.[22] Ultrafast laser excitation impulsively excites the lowest frequency "breathing" mode of the particles, which gives rise to a beat signal in our transient absorption experiments. A second goal of this review is to describe in detail the assignment of this signal, and how the pump laser induces the coherent vibrational motion.

The creation and detection of vibrational coherence is an integral part of time-resolved studies of isolated molecules, condensed phase samples, as well as biological systems.[23−25] These experiments are capable of providing dynamical information that cannot be obtained by conventional spectroscopic techniques. Thus, vibrational coherence measurements have become a major tool in physical chemistry laboratories. In general, vibrational coherence can be observed whenever the impulse that drives the nuclear motion is faster than the characteristic time scale for vibration. In molecules this impulse is usually supplied by a short laser pulse that excites the molecule from its ground electronic state to a higher state with a different geometry.[23−25] This produces a wave packet that evolves in time, and gives a quantum beat signal in transient absorption experiments. It will be shown that the modulations observed in our experiments arise from a very different excitation mechanism, and that they can be completely understood with classical mechanics—unlike the coherent nuclear response in semiconductors and molecules.

An important part of this work is the preparation of high quality metal particle samples. These samples are made by reducing metal ions in aqueous solution, using both chemical and radiation chemistry techniques.[26] In particular, radiation chemistry offers several advantages for producing metal particles: (i) The particles are prepared without the presence of strongly adsorbed capping agents, such as thiols. This is particularly important in spectroscopic studies, since the plasmon band (which dominates the absorption spectrum for small metal particles) is very sensitive to the environment around the particle. (ii) The solutions do not contain the remnants of the reducing

* To whom correspondence should be addressed. E-mail: hartland.1@nd.edu.
[†] Department of Chemistry and Biochemistry.
[‡] Radiation Laboratory.

10.1021/jp002256x CCC: $19.00
Published on Web 09/28/2000

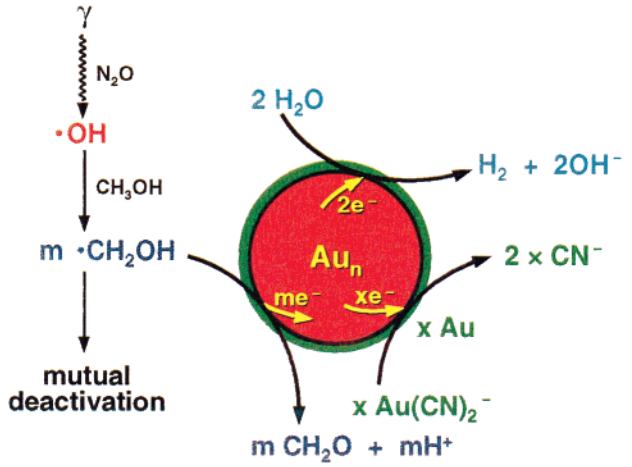

Figure 1. Enlargement of colloidal gold particles via radiation chemistry. The gold seed particles store electrons, which subsequently reduce $Au(CN)_2^-$ onto the particle surface. The reduction of water by the stored electrons is a competing reaction.

molecules and are also photochemically stable, unlike thiol derivatized metal particles. (iii) Single component metal particles of any desired size,[27] and core−shell bimetallic particles with cores and shells of any dimension, can be produced using radiation chemistry.[28−31] The core−shell particles in particular are unique, and understanding their properties is a major component of our research efforts.

Experimental Techniques

Preparation of Metal Colloids. The ions of all noble metals, as well as of many electronegative metals, can be reduced by exposing their aqueous solutions to γ-radiation.[26] To all practical purposes the absorption of radiation only occurs in the solvent—due to the much higher concentration of the solvent compared to the solute. Reducing free radicals, aqueous electrons and hydrogen atoms, as well as oxidizing ·OH radicals are generated. These species subsequently attack any dissolved substances. To achieve overall reduction of a metal ion (generally at a concentration of 10^{-4} to 10^{-3} M), an alcohol in much higher concentration (ca. 0.1 M) is added. The alcohol scavenges the ·OH radicals by the reaction $\cdot OH + CH_3OH \rightarrow H_2O + \cdot CH_2OH$, for example, and the organic radicals produced also act as reductants. The redox properties of these species are very well-known, thus, one can select a free radical to perform a desired action. In some cases it is useful to only produce organic radicals (i.e., to eliminate all primary radicals from water radiolysis). This is achieved by irradiating under an atmosphere of nitrous oxide. The hydrated electrons are scavenged by the reaction: $N_2O + e_{aq}^- + H_2O \rightarrow N_2 + OH^- + \cdot OH$, and the ·OH radical then reacts with the alcohol to produce additional organic radicals. The formation of radicals occurs uniformly in solution, in contrast to photochemical experiments. Thus, the reduction of metal ions can be carried out in a highly controlled manner through radiation chemistry.

An important use of radiation chemistry is to grow existing nanoparticles into larger ones.[27] Figure 1 shows the reaction scheme for making different sized Au particles. A solution containing Au seed particles, potassium dicyano-aurate-I, methanol and nitrous oxide is γ-irradiated, producing 1-hydroxymethyl radicals. These radicals cannot reduce Au−I complexes in solution, as this reaction is highly endoergic due to the large free energy of formation of a free Au atom. Thus, the radicals are left to react with the colloid particles by transferring an electron. A colloidal particle can react with many radicals, which means it can store a large number of electrons.[32] The Au particle thus becomes a tiny cathode, and the stored electrons are able to reduce $Au(CN)_2^-$ directly onto the surface of the particle.[27] Irradiation is carried out until all the Au−I complex is reduced, and the final size of the particles is simply determined by the amount of gold complex used. After irradiation the solutions contain CN^- ions, which can be readily removed by treating the solution with ion-exchange resin. The seed particles are typically made using the conventional citrate reduction method.[33]

The above technique can also be used to prepare composite metal particles of the core−shell type.[28−31] For example, when $Ag(CN)_2^-$ is used instead of the gold complex in Figure 1, a Ag shell is formed around the Au particle. Figure 2 shows a typical electron micrograph of the $Au_{core}Ag_{shell}$ particles produced by radiation chemistry, as well as a micrograph of the original seed particles. The Ag shell can be clearly distinguished

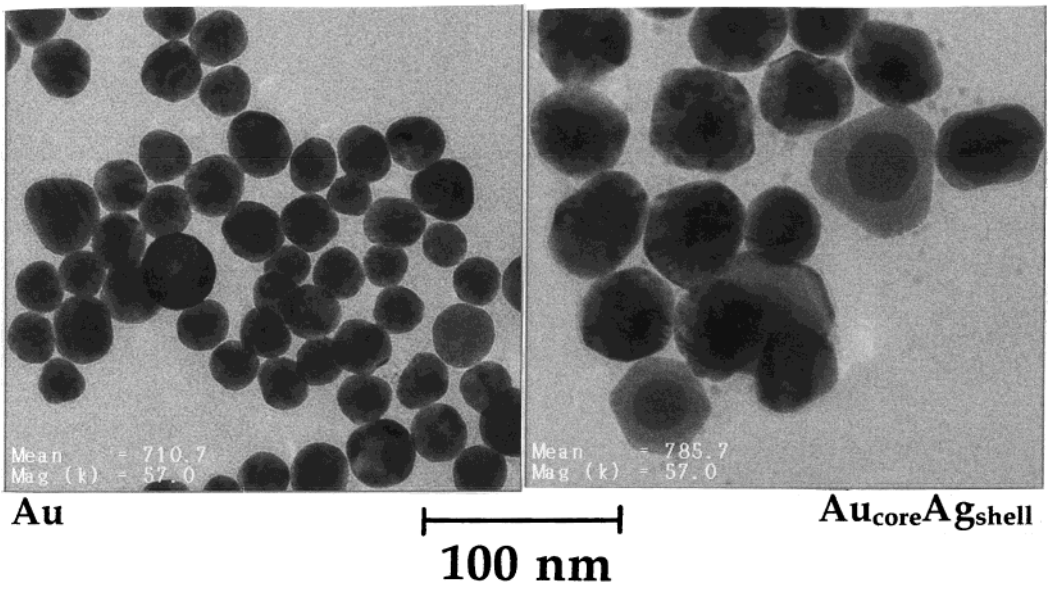

Figure 2. TEM micrographs of 20 nm diameter Au particles prepared using the Turkevich method (left), and after coating with Ag (right). The molar ratios are Au:Ag = 1:1. The Ag coating is not always uniform, and in some cases the Ag shell grows into a large crystal surrounding the Au nucleus.

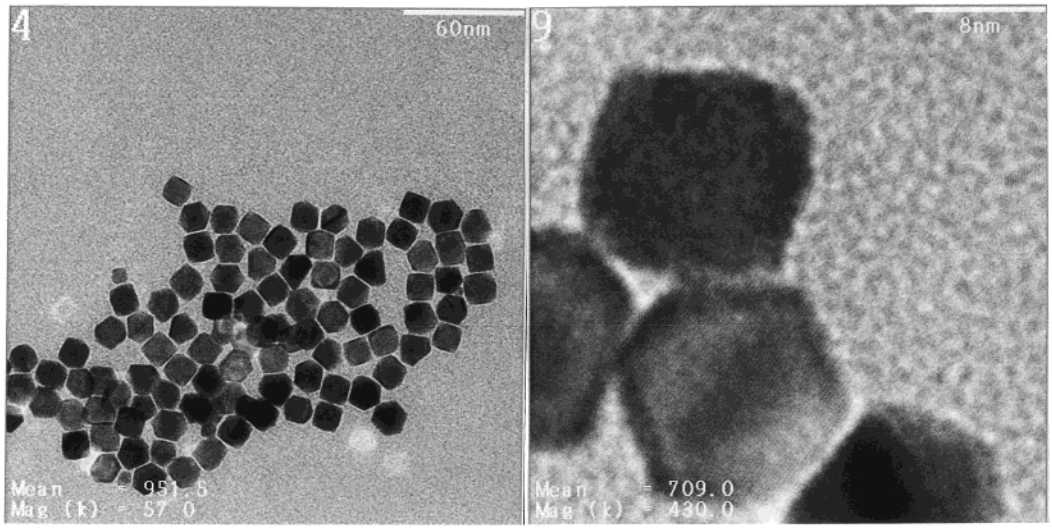

Figure 3. TEM micrographs of Pt particles produced by reduction of 5×10^{-4} M $PtCl_2(H_2O)_2$ by H_2, in the presence of 5×10^{-4} M sodium citrate and 5×10^{-4} M NaOH. At higher resolution the lattice planes of Pt can be seen. These perfectly run through the whole nanocrystal, showing that these particles are essentially defect free.

by TEM. These preparations have to occur under strict exclusion of air. However, the particles of noble metals which result are generally stable toward air. No special precautions have to be taken, therefore, in the photophysical experiments. This is not true for particles that contain nonnoble metals. For example, for $Au_{core}Pb_{shell}$ particles the Pb shell is dissolved within seconds when the solution is exposed to air.[29] Rigorous exclusion of air is therefore essential for photophysical experiments with these particles. Some of the data discussed below involved platinum particles, which were made by reduction of $PtCl_2(H_2O)_2$ by hydrogen with citrate as a stabilizer.[34] Hydrogen is an excellent reducing agent as it leaves no undesirable byproducts in solution. Figure 3 shows an electron micrograph of the Pt particles obtained by this method. They have a narrow size distribution and consist mainly of cubic and cuboctahedral crystals.

Transient Absorption Apparatus. The transient absorption experiments were performed using a pump−probe scheme: a pump laser pulse is used to excite the sample and a second, variably delayed probe pulse is used to monitor its time-evolution. In our experiments both the pump and probe pulses are obtained from a regeneratively amplified Ti:sapphire laser system (Clark-MXR, CPA-1000). This laser produces pulses in the 780−820 nm range with a full width at half-maximum of 120−150 fs ($sech^2$ deconvolution), and an energy of 400−500 mJ per pulse. The output is split by a 90:10 beam splitter to create the pump and probe beams. The timing between the two laser pulses is controlled by a stepper motor driven translation stage (Newport, UTM150PP.1). For the experiments described below, the pump was frequency-doubled in a 1 mm BBO crystal before the sample. Visible probe laser pulses were obtained from a white-light continuum generated in either a 3 mm sapphire window or a 1 cm cuvette of water. The pump and probe were spatially overlapped at the sample, and the transmitted probe intensity was monitored by a Si−PIN photodiode (Thorlabs, PA150). A normalization scheme using gated integration, an analogue division circuit, and lock-in detection of the signal was used to reduce noise due to fluctuations in the probe laser.[19] For some of our experiments the metal particle samples were flowed through a 3 mm path length sample cell. The air-sensitive samples were kept in sealed cuvettes. These experiments were performed without flowing, and the pump laser intensity was reduced to avoid thermal lensing effects.

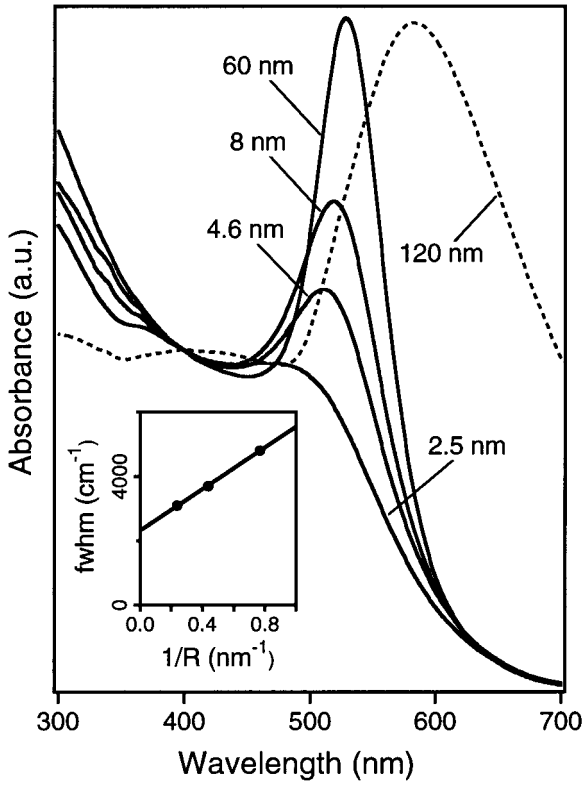

Figure 4. Extinction spectra of the different sized Au particles in aqueous solutions with a Au concentration of 2×10^{-4} M. The inset shows the full width at half-maximum of the plasmon band for the 2.5, 4.6, and 8 nm diameter particles.

Photophysics and Electron−Phonon Coupling in Au Particles

Before discussing the breathing mode experiments, it is important to describe the spectroscopy of metal particles, and the sequence of events that occur following excitation by an ultrafast laser pulse. Figure 4 shows the absorption spectra of different sized Au particles, with diameters ranging from 2.5 to 120 nm. The visible region of the spectrum is dominated by the plasmon band, which is a collective oscillation of the conduction band electrons across the particle.[35−38] For particles larger than ca. 10 nm the position and shape of the plasmon

band can be described by classical electrodynamics (Mie theory), taking into account absorption and scattering contributions to the extinction cross-section.[35−37] For particles smaller than ca. 60 nm only the absorption term is important, and the cross-section is given by the equation[37]

$$\sigma(\omega,T) \propto \epsilon_m^{3/2} \frac{\omega\epsilon_2(\omega)}{[\epsilon_1(\omega) + 2\epsilon_m]^2 + \epsilon_2(\omega)^2} \quad (1)$$

where ϵ_m is the dielectric constant of the medium, and $\epsilon_1(\omega)$ and $\epsilon_2(\omega)$ are the real and imaginary components of the dielectric constant of the metal—which implicitly depend on the temperature.[39] Equation 1 can satisfactorily reproduce the absorption spectra as long as the dielectric constants are accurately known. The broadening and red-shift in the plasmon band for the larger 120 nm diameter particles (see Figure 4) is primarily due to an increased contribution from scattering to the extinction coefficient.[35,37]

For particles smaller than ca. 10 nm the plasmon band becomes broader and shifts to the blue. The broadening can be qualitatively explained by considering how electron-surface scattering contributes to the dieletric constant.[37] Specifically, the dielectric constant contains contributions from interband transitions and from intraband transitions:[40,41]

$$\epsilon_1(\omega) = \epsilon_1^{intra}(\omega) + \epsilon_1^{inter}(\omega)$$
$$\epsilon_2(\omega) = \epsilon_2^{intra}(\omega) + \epsilon_2^{inter}(\omega) \quad (2)$$

The intraband contribution can be calculated using the Drude model:[41]

$$\epsilon_1^{intra} = 1 - \frac{\omega_p^2}{\omega^2 + \Gamma^2}$$
$$\epsilon_2^{intra} = \frac{\omega_p^2\Gamma}{\omega(\omega^2 + \Gamma^2)} \quad (3)$$

where ω_p is the plasma frequency (a fundamental property of the metal) and Γ is a damping constant. For metals such as Al and Ag, where the onset of the interband transitions is well separated from the plasmon band, the bandwidth is controlled by Γ.[37] For metals such as Au and Cu where the interband transitions occur in the same spectral region as the plasmon band, the bandwidth is determined by both Γ and the frequency dependence of $\epsilon^{inter}(\omega)$. This makes the analysis more difficult. However, in either case the way the bandwidth changes with size can be accounted for by writing[37,42−44]

$$\Gamma = \Gamma_0 + A\frac{\upsilon_F}{R} \quad (4)$$

where R is the particle radius, υ_F is the Fermi velocity of the electrons, and A is a constant on the order of unity. The first term in eq 4 describes the bulk contribution to the dephasing of the electrons, and the second term accounts for the additional dephasing due to electron-surface scattering. The exact value of A depends on how the electron-surface interaction is modeled.[37,43]

The inset of Figure 4 shows how the width of the plasmon band varies with $1/R$ for Au particles with diameters between 2 and 8 nm. Note that the polydispersity in the samples does not significantly affect these measurements, because the position of the plasmon band is only weakly dependent on the particle size.[27,45−47] A straight-line fit to the data in Figure 4 yields $A = 0.43$ and $\Gamma_0 = 4.4 \times 10^{14}$ Hz, which implies an intrinsic (bulk) electronic dephasing time of 2.3 fs. These results are in good agreement with previous studies of the plasmon band of Au, and show that electron-surface scattering is primarily responsible for the broadening of the plasmon band observed for the smaller particles.[37] The blue shift in the plasmon band for the 2.5 nm diameter particles is attributed to size dependent changes in the dielectric function.[46]

In our transient absorption experiments a 400 nm laser pulse is used to excite the sample. For Au this color predominantly excites 5d → 6sp interband transitions; i.e., electrons are promoted from the filled 5d band to empty states above the Fermi level in the 6sp band.[40,41] The energy deposited by the pump laser is rapidly equilibrated (<200 fs) among all the conduction band electrons by e−e scattering.[48−52] For pure Ag and Au particles these processes occur before any significant energy exchange between the electrons and phonons. Thus, shortly after laser excitation the electrons and phonons have different temperatures. Because electrons have a very small heat capacity, increases in the electronic temperature of several thousand *K* can be easily achieved by ultrafast laser excitation. This changes the occupation of the electronic states near the Fermi level which, in turn, affects the interband contribution to the dielectric constant.[39] The changes to $\epsilon_1^{inter}(\omega)$ and $\epsilon_2^{inter}(\omega)$ broaden the plasmon band, which creates a strong bleach signal at the band maximum and absorption signals in the wings of the band.[14,19] The magnitude of the bleach is proportional to the electronic temperature.[19] As time progresses the electrons equilibrate with the lattice via e−ph coupling.[12−21] This process can be monitored by measuring either the recovery of the bleach or the decay of the transient absorption signal.[14,19]

Figure 5a shows an example of transient bleach experiments for 11 ± 2 nm diameter Au particles. These experiments were performed with the probe laser tuned to the peak of the plasmon band (520 nm). This wavelength corresponds to the maximum transient bleach signal and, therefore, yields the highest sensitivity. There are two important points to note: First, the low power experiments can be fitted to a single-exponential decay, which allows us to define a characteristic cooling time for the electrons.[19] Second, the cooling time depends on the pump laser power. This can be understood through the two-temperature model,[53−57] which describes the energy exchange between the electrons and phonons by the coupled equations

$$C_e(T_e)\frac{\partial T_e}{\partial t} = -g(T_e - T_l)$$
$$C_l\frac{\partial T_l}{\partial t} = g(T_e - T_l) \quad (5)$$

where T_e and T_l are the electronic and lattice temperatures, $C_e(T_e) = \gamma T_e$ is the temperature-dependent electronic heat capacity, $\gamma = 66$ Jm^{-3} K^{-2} for Au,[41] C_l is the lattice heat capacity, and g is the e−ph coupling constant. When the temperature change in the electron gas is small (i.e., at low pump power) the relaxation time is given by $\gamma(T_0 + \Delta T)/g$, where T_0 is the ambient temperature and ΔT is the temperature increase induced by the pump laser.[19] Thus, the increase in relaxation time with pump laser power is simply due to higher initial electronic temperatures.

The power dependence of the transient bleach signal makes it extremely difficult to define a characteristic time scale for e−ph coupling.[14,19] Our approach to this problem is to perform a series of measurements at different pump laser powers, and extrapolate the measured time constants to zero power.[19] An

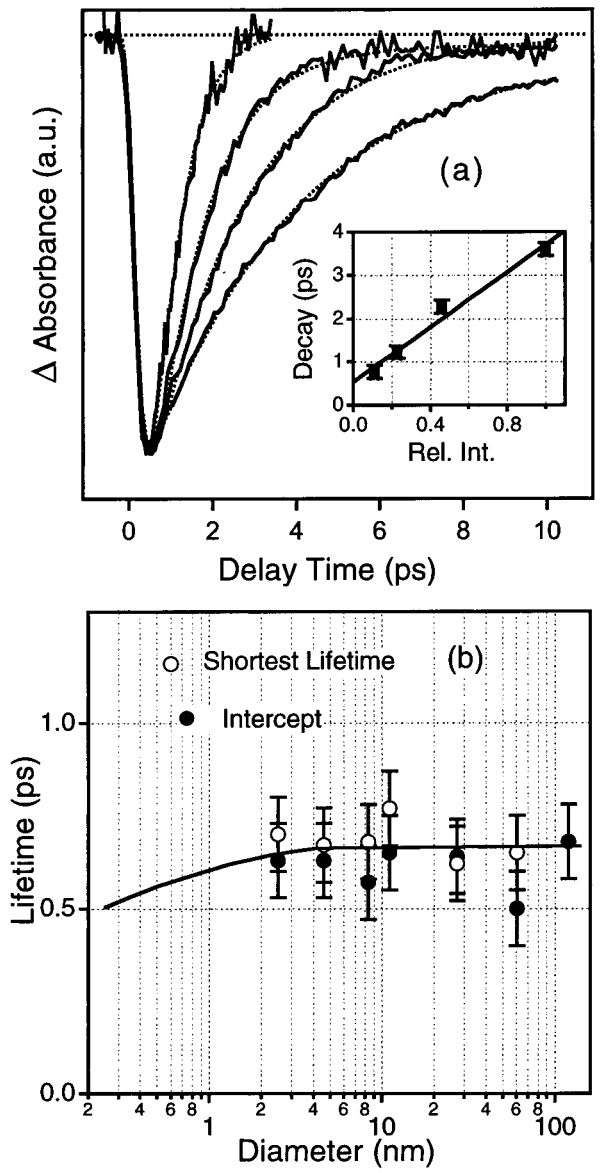

Figure 5. (a) Transient absorption data for 11 ± 2 nm diameter Au particles. The different traces have been normalized by their maximum bleach signal at ca. 0 ps delay. The inset shows a plot of the measured decay times versus the relative pump laser power. (b) Characteristic e−ph coupling time versus diameter for Au. The solid line is a plot of the calculated e−ph coupling time; see text for details.

example of this procedure is shown in the inset of Figure 5a, where the measured time constants are plotted versus relative pump laser intensity (the maximum pump power used was ∼0.3 mJ/pulse). The intercept is given by $\gamma T_0/g$. Figure 5b shows the characteristic e−ph coupling times measured for a series of Au samples plotted against the particle diameter.[19] Both the intercepts obtained from the extrapolation procedure, and the fastest measured decay times (which correspond to the smallest experimental values of ΔT) are presented. The conclusion from these experiments is that time scale for e−ph coupling does not depend on particle size, for samples in the 2.5 nm to 120 nm diameter range.[19] Furthermore, the e−ph coupling times are similar to the 0.65 ps time constant measured for bulk Au.[55]

These results can be explained in the following way. The relaxation of the hot electron gas occurs through two different channels: bulk e−ph coupling and electron-surface coupling. The electron-surface coupling arises from interactions between the electrons and either the acoustic or the capillary surface vibrational modes.[57] The acoustic modes change the particle volume, while the capillary modes affect the shape without changing the volume. Since these mechanisms occur in parallel, the effective e−ph coupling constant is given by[19]

$$g_{\text{eff}} = g_{\text{bulk}} + g_{\text{a}}(R) + g_{\text{c}}(R) \tag{6}$$

where the last two terms stand for the acoustic and capillary surface mode coupling terms, respectively. The values of $g_{\text{a}}(R)$ and $g_{\text{c}}(R)$ can be calculated using the theory developed by Belotskii et al.[57] In this model the electron gas is assumed to be contained in a spherical potential well with the dimensions of the particle, and a depth V_0 equal to the Fermi energy.[15] The values of $g_{\text{a}}(R)$ and $g_{\text{c}}(R)$ are given by

$$g_{\text{a}}(R) = \frac{1}{16\pi}\frac{v_{\text{F}}}{R^2}k_{\text{B}}n\frac{m_{\text{e}}}{\rho}\left(\frac{\omega_{\text{D}}}{c_{\text{l}}}\right)^2\left(\frac{V_0}{\varphi_0}\right)^2 \tag{7a}$$

$$g_{\text{c}}(R) = \frac{3}{16\pi}\frac{v_{\text{F}}}{R}k_{\text{B}}n\frac{m_{\text{e}}\omega_{\text{l}}^2}{\sigma}\left(\frac{V_0}{\varphi_0}\right)^2 \tag{7b}$$

where k_{B} is Boltzmann's constant, m_e is the electron mass, ρ is the metal density, n is the free electron density, ω_{D} is the Debye frequency, c_{l} is the longitudinal speed of sound, φ_0 is the work function of the metal, σ is the surface tension, and ω_{l} is the maximum frequency of the capillary modes.[15,19,57] The solid line in Figure 5b shows the characteristic e−ph coupling time, $\gamma T_0/g_{\text{eff}}$, calculated using these expressions. The bulk contribution was assumed to be $\gamma_{\text{bulk}} = 2.95 \times 10^{16}$ W m^{-3} K^{-1}, which is the value measured by Groeneveld et al.[55] These calculations show that for Au particles larger than 1 nm diameter $g_{\text{a}}(R) + g_{\text{c}}(R) \ll g_{\text{bulk}}$, which means that g_{eff} is independent of size.

Nisoli and co-workers showed that the model of Belotskii et al. almost exactly accounts for the variation in relaxation time with size for gallium nanoparticles with diameters between 10 and 18 nm.[15] We have used this model to calculate g_{eff} for Ag particles with diameters between 4 and 30 nm, and find that it accounts for ca. 50% of the change in the relaxation time measured experimentally.[18] Thus, the predictions of this theory are in good agreement with the available experimental data for Ga, Ag and Au nanoparticles. What appears to determine the magnitude of the surface coupling term for different metals is the ratio of the electron density to the metal density (n/ρ), which is proportional to the valence of the metal divided by its atomic mass. Thus, Au which has high atomic mass ($n/\rho = 3.1 \times 10^{21}$ g^{-1}), has a smaller electron-surface coupling than Ga ($n/\rho = 2.6 \times 10^{22}$ g^{-1}) or Ag ($n/\rho = 5.6 \times 10^{21}$ g^{-1}). The physical picture that emerges is that electron-surface collisions will not significantly displace the surface atoms from their equilibrium position for heavy elements, such as Au. This means that the surface phonon modes will not be efficiently excited, and there will be little energy transfer from the electrons to these modes. For metals with a large free electron density, such as Ga, the frequency of electron-surface collisions is larger, which increases the probability of energy transfer. Likewise, metals with lighter nuclei will have larger surface contributions to the e−ph coupling constant.

Coherent Excitation of Acoustic Phonon Modes

The above results show that the energy deposited into the particles by laser excitation flows into the phonon modes on a picosecond time scale (the exact time depends on the initial electronic temperature). This energy is eventually dissipated to the solvent. However, for a short time (<200 ps) the lattice

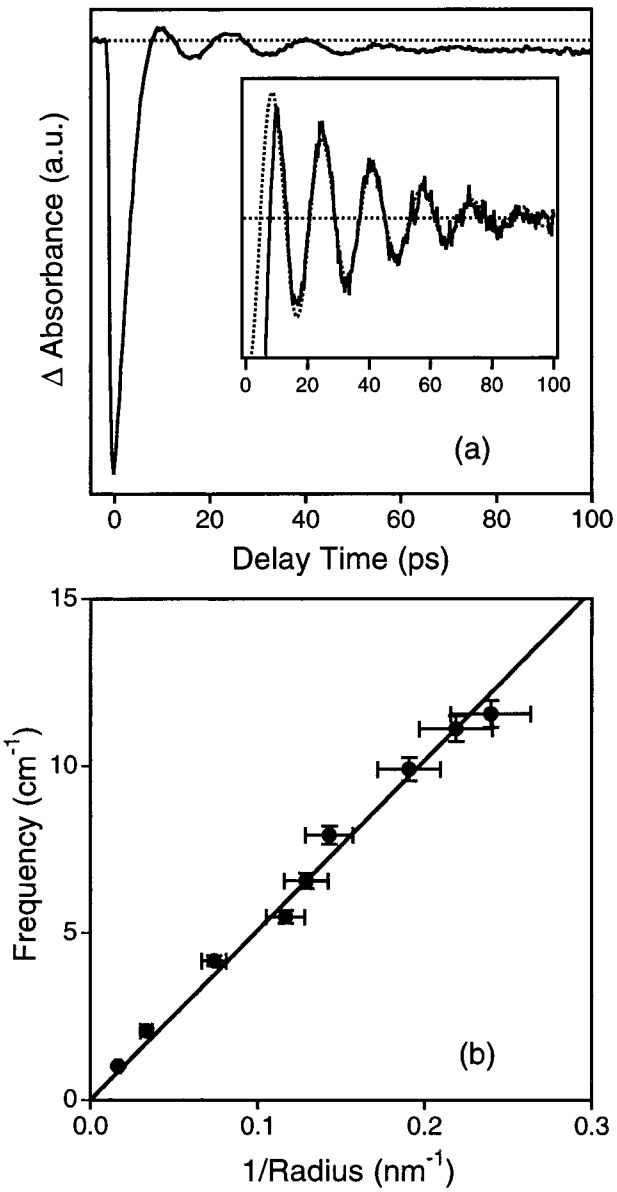

Figure 6. (a) Transient absorption data for 60 nm diameter Au particles recorded with 400 nm pump and 550 nm probe pulses. Modulations due to the coherently excited breathing motion can be clearly seen. (b) Plot of the measured frequencies versus 1/*R* for different Au samples. A straight line fit to the data is also shown.

suffers a significant increase in temperature, which causes it to expand. If the time scale for heating is faster than the period of the collective phonon mode that corresponds to expansion, then this mode can be impulsively excited.[22,58−62] Figure 6a shows an experimental trace that contains an oscillating signal due to the coherently excited phonon modes. The average diameter of the particles in this sample was 60 nm, and the probe wavelength used was 550 nm (i.e., on the red side of the plasmon band). The dashed line in Figure 6a is a fit to the data using a damped cosine function $S(t) = A_0 \cos(2\pi c\bar{\nu}_R t + \phi)e^{-t/\tau}$, where $\bar{\nu}_R$ is the frequency (in cm^{-1}), ϕ is the phase and τ is a constant that accounts for the damping of the modulations. The excellent fit to the experimental data shows that the oscillation only contains a single frequency. The measured frequencies are strongly dependent on the particle size.[59,60] Figure 6b shows a plot of the frequency versus 1/*R*, for a range of different Au particle samples. The frequency changes from 1.0 cm^{-1} for 120 nm diameter particles, to 11.6 cm^{-1} for 8.3 nm diameter particles. The data can be well fitted to a straight line with a formula $\bar{\nu}_R = (50.75 \pm 0.95)/R$, for *R* in nm.[59] Similar modulations have been observed for for Ga and Sn particles grown on a surface,[58] Ag particles embedded in a glass,[60] and Au particles grown in a semiconductor matrix.[61]

The frequency and form of the vibrational modes of spherical particles have been calculated using classical mechanics.[63,64] Two different types of vibrations exist: torsional modes (which have no displacement along the radial direction) and spheroidal modes (which have displacements along both the radial and transversal directions).[63,64] These modes are characterized by two integers—a solution number and an angular momentum number *l*. The lowest order spheroidal modes ($l = 0$) only involve radial motion.[63,64] These "breathing modes" are the ones expected to be excited by the isotropic heating/expansion process. The frequencies of the $l = 0$ spheroidal modes are given by[63,64]

$$\bar{\nu}_R = \frac{\eta c_l}{2\pi R c} \tag{8}$$

where η is an eigenvalue, c is the speed of light, and the longitudinal speed of sound c_l is 3240 ms^{-1} for Au. For an isolated sphere the eigenvalues for the $l = 0$ modes are given by the roots of the equation[63,64]

$$\eta \cot \eta = 1 - \frac{\eta^2}{4\delta^2} \tag{9}$$

where $\delta = c_t/c_l$ is the ratio of the transversal and longitudinal speeds of sound. For Au this calculation yields $\eta = 2.93$ for the lowest frequency radial mode. In comparison, our experimental data yields $\eta = 2.95 \pm 0.06$.[59] The excellent agreement between the calculated and experimental values of η confirms that the observed oscillations are due to the symmetric breathing mode of the particles. It is remarkable that these formulas, which were first developed over one hundred years ago and only involve the bulk elastic properties of Au, account for the response of nanometer sized particles on a picosecond time scale!

The coherently excited breathing motion contributes to our transient absorption experiments because changes in the particle size change the position of the plasmon band.[22,59] For a free-electron metal (i.e., where the dielectric constant can be accurately described using eqs 3) the maximum of the plasmon band occurs at

$$\omega_{max} = \frac{\omega_p}{\sqrt{1 + 2\epsilon_m}} \tag{10}$$

where the plasma frequency ω_p is

$$\omega_p = (ne^2/\epsilon_o m_e)^{1/2} \tag{11}$$

where ϵ_o is the vacuum permittivity, and e is the electron charge.[41] Note that only considering the free electron contribution to the dielectric function is a drastic approximation for Au, however, these equations correctly describe the physics behind the modulations. Equations 10 and 11 show that changes in the free electron density will change ω_p and, therefore, the position of the plasmon band. Thus, the coherently excited breathing motion, which modulates the particle volume, will cause the plasmon band to shift back-and-forth. This creates an oscillation in our transient absorption signal.[22,59] By comparing to calculated transient absorption spectra, we estimate that the free electron

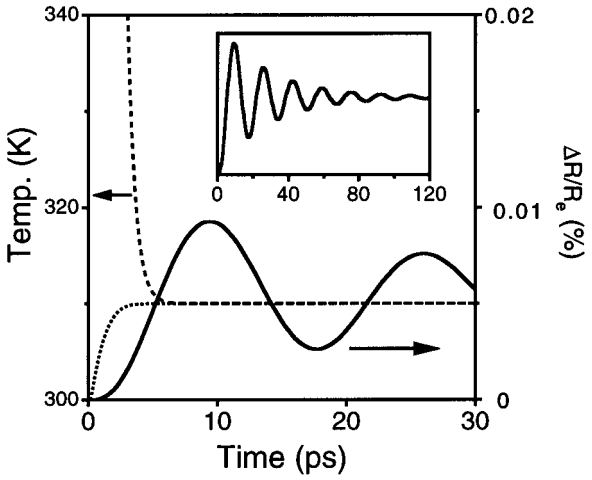

Figure 7. Calculated change in the radius (—) and electronic (- - -) and lattice (···) temperatures for a 60 nm diameter Au particle with an initial electronic temperature of 3000 K. The inset shows $\Delta R/R_e$ over a longer time range.

density has to change by <0.4% to account for the magnitude of the oscillations.[22,59] This analysis predicts that modulations recorded with the probe laser tuned to the red or blue sides of the plasmon band should be out-of-phase with respect to each other. This has been observed for Ag particles by Del Fatti et al.[60] Unfortunately, we have not been able to observe modulations with the probe laser tuned to the blue of the plasmon band for our Au samples.

Assuming that the breathing vibration can be treated as a harmonic oscillator, the response of the particles to heating can be modeled using the following equation:[59,60]

$$\frac{d^2R}{dt^2} + \frac{2}{\tau}\frac{dR}{dt} + (2\pi c\bar{\nu}_R)^2\{R - [R_e + \Delta R_e(T_l)]\} = 0 \quad (12)$$

where τ is a damping time, R_e is the equilibrium radius at room temperature, and $\Delta R_e(T_l)$ is the increase in the radius caused by the increase in the lattice temperature. For small temperature increases $\Delta R_e(T_l)$ is given by

$$\Delta R_e(T_l) = \frac{R_e\alpha}{3}(T_l - 298) \quad (13)$$

where α is the coefficient of thermal expansion for the metal. Figure 7 shows a plot of the electronic and lattice temperatures, and $(R - R_e)/R_e$ versus time for a 60 nm diameter Au particle with an initial electronic temperature of 3000 K. The time dependence of the electronic and lattice temperatures was calculated using eq 5. Note that the only adjustable parameter in these calculations is the damping time, which was set to match the experimentally observed decay. All the other parameters—α, $\bar{\nu}_R$, C_e, C_l and g—were taken from the literature.[59]

The results of these calculations can be physically explained as follows: Heat flows from the electrons into the lattice on a time scale of ca. 2 ps. The increase in lattice temperature increases the equilibrium radius from R_e to $R_e + \Delta R_e(T_l)$; i.e., it shifts the minimum of the potential energy curve that describes the breathing motion. For Au particles larger than ca. 8 nm the frequency of the breathing mode is slower than the time scale for heating. Thus, the change in the equilibrium radius is "sudden" compared to the response time of the nuclei. When the damping time for the breathing motion is longer than the period, the system will oscillate around the new equilibrium radius. Figure 7 shows that for an initial electronic temperature of 3000 K, the equilibrium radius of the particles increases by ca. 0.005% and the maximum expansion is slightly less than 0.01%. It is interesting to note that both the mechanism for generating the beat signal, and the observed frequencies can be explained purely by classical mechanics.

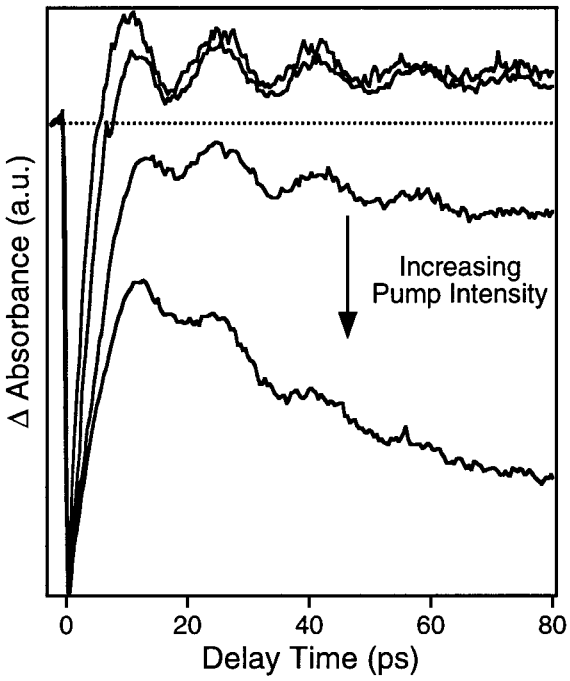

Figure 8. Transient absorption data for 60 nm diameter Au particles recorded with different pump laser powers. The data have been normalized by the maximum bleach signal at ca. 0 ps. Note that the time scale for the initial bleach recovery increases and the relative magnitude of the modulation decreases as the pump laser power increases.

Equations 12 and 13 allow us to predict how the signal should change as we vary the pump laser power, i.e., as we change the initial electronic temperature. Higher electronic temperatures give larger lattice temperatures and, therefore, greater expansion. However, the time scale for e−ph coupling also increases, as shown in Figure 5, so that lattice heating is no longer sudden compared to the period of the breathing mode. The overall result is that the magnitude of the modulations relative to the initial bleach signal actually decreases as the pump laser power increases.[59] Experimental data that shows this effect is presented in Figure 8. The pump laser power was varied from 1 to 5 μJ/pulse in these experiments, and the data have been normalized by their peak signal near $\tau = 0$ ps. For very small particles the vibrational period is similar to the lattice heating time, even at the lowest pump laser powers that can be used. Thus, the particles expand and contract several times while heat is being fed into the lattice, which washes out the coherent breathing motion. Because of this we have not been able to observe modulations for Au particles smaller than 8 nm diameter.

An interesting question in these experiments is what causes the decay in the modulations? Several mechanisms are possible, for example, coupling to other phonon modes, energy exchange with the environment, or dephasing due to the spread of sizes in the sample (different sized particles have different breathing mode frequencies). The first mechanism is unlikely because the breathing mode is the lowest frequency vibration of the particle; i.e., there are no lower energy phonon modes to accept the energy. The contribution from the last mechanism can be estimated by comparing the experimental data to a sum of weighted cosine functions:

$$S(t) = \sum_i A_i \cos(\eta c_l t/R_i + \varphi) \quad (14)$$

where the coefficients A_i are determined by the abundance of particles with a radius R_i in the sample, and the phase φ is an adjustable parameter (that does not depend on size). The decays predicted using this equation almost exactly match those measured experimentally (the weighting coefficients were determined from TEM measurements).[59] Thus, the dephasing of the oscillations in our data is controlled by the polydispersity of the samples, and not by energy transfer to the surrounding medium. More oscillations will be observed for samples with narrower size distributions. For aqueous colloidal systems we have been able to observe up to six periods—see Figure 6. On the other hand, over eight periods have been observed for Au nanoparticles grown in a TiO_2 thin film, indicating that these samples have a very narrow size distribution.[61]

Modulations due to coherently excited breathing modes have also been observed in transient absorption experiments with semiconductor particles.[65,66] In this case promotion of electrons from the valence band to the conduction band reduces the screening between nuclei, which increases the size of the unit cell.[67] This sudden displacement impulsively excites the symmetric breathing mode.[65,66] This mechanism is analogous to how quantum beats are generated in molecules (i.e., optical excitation to an electronic state with a different equilibrium geometry). However, it is not relevant for metal particles: in metals the lifetimes of the excited electronic states are too short to allow significant displacement of the low frequency phonon modes. In our experiments expansion occurs via heat transfer from the excited electrons to the phonons. Thus, for semiconductor particles the only fundamental limitation for coherently exciting the breathing motion is the laser pulse width, whereas, for metal particles it is the e−ph coupling time. In addition, for semiconductors increasing the pump laser power leads to a greater change in the charge carrier density in the conduction band, which produces a larger increase in the unit cell dimensions.[67] This means that the relative amplitude of the coherent vibrational motion increases with pump laser power (at least until the particles melt or suffer fragmentation).[65,66] In contrast, as shown above, for metal particles increasing the pump laser power washes-out the coherent nuclear response. Because of this, the vibrational amplitudes that can be achieved in semiconductors are larger than those for metal particles.

Our experiments are similar in spirit to transient grating/reflectivity studies of thin films.[68,69] In these experiments surface acoustic waves that propagate in the plane of the film, and/or longitudinal waves that travel perpendicular to the surface, are generated by ultrafast laser excitation.[68] These waves are launched by the thermal expansion that accompanies optical excitation and e−ph coupling. The longitudinal waves take the form of an acoustic pulse that propagates through the film, and is reflected at the film/substrate interface. When this pulse returns to the surface it creates a transient signal that is detected by the probe laser pulse.[68] Similarly, the surface acoustic waves create a "ripple" at the film surface that affects the diffraction of the probe beam.[68] Both the frequencies of the surface acoustic waves and the transit time for the through-plane acoustic pulse provide information about the mechanical properties and thickness of the film, and a commercial device based on this technique has been produced to interrogate thin films on semiconductor surfaces.[69] The modulations observed in our experiments represent the limit of what would happen to the surface acoustic waves if one took a thin metal film and chopped it up into small pieces.

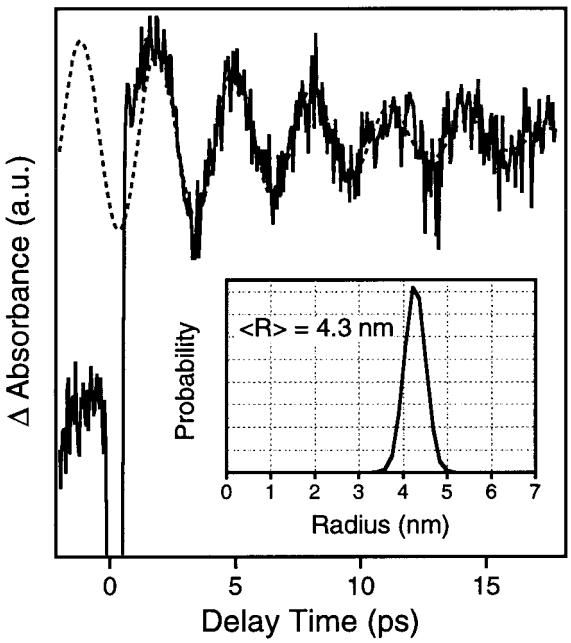

Figure 9. Transient absorption data for Pt particles recorded with 400 nm pump and 512 nm probe pulses. The dashed line is a fit to the data obtained using eq 14 and the inset shows the size distribution obtained from the fitting procedure.

In Situ Measurements of the Particle Size Distribution. The successful use of time-resolved spectroscopy to analyze thin films suggests that our experiments might be useful for measuring particle size distributions.[70] In fact, there are several advantages of these experiments compared to TEM or STM measurements. First, because the experiments are all optical, measurements can be made in situ for virtually any environment. This is a big advantage for air sensitive or unstable samples, which might be destroyed by preparing a TEM grid. Second, transient absorption experiments interrogate 10^4-10^8 particles, depending on the size of particles and the exact conditions used. In contrast, TEM or STM measurements interrogate $10-10^2$ particles. Thus, the results from transient absorption experiments are statistically more reliable. Third, these measurements can be applied to any metal, as long as the transverse and longitudinal speeds of sound are known.

Figure 9 shows transient absorption data for a Pt particle sample recorded with 400 nm pump and 512 nm probe pulses. Note that the acoustic modulations can be observed with visible probe laser pulses, even though the plasmon band for Pt occurs in the UV. However, typically we find that the strongest beat signals are observed near the plasmon band. Furthermore, the observation of 5−6 periods implies a fairly narrow size distribution. The dashed line in Figure 9 was obtained from eq 14, using values of η and c_l determined from data in ref 71. The coefficients for the cosines were assumed to have a normal distribution, and a least-squares fitting routine was used to adjust the average radius $\langle R \rangle$ and width σ of the size distribution to best fit the data. The results are shown in the inset of Figure 9. TEM pictures of the same Pt particle sample are shown in Figure 3. Note that the average diameter of 13 ± 2 nm determined from the TEM measurements, is much bigger than that calculated from the transient absorption data (9 ± 2 nm). This error (~30%) is significantly larger than that for the Au samples, which gave almost perfect agreement between the TEM and transient absorption results (see Figure 6). We believe that the major reason for this discrepancy is that the Pt particles are not spherical, and the acoustic modes for nonspherical particles are

very different to those for spheres.[72] Thus, our experiments only give qualitative information for nonspherical particles.[70] On the other hand, the results are much more accurate than those from other optical techniques, such as dynamic light scattering or analysis of the UV−vis absorption spectra (unlike semiconductors, such as CdSe, it is difficult to extract size information from the absorption spectra of metal particles). Thus, the experiments described above could be useful for measuring size distributions of metal particle samples when quick, in-situ measurements are needed.

Core−Shell Nanoparticles

A significant question in these experiments is whether the frequency and/or the damping time of the beat signal depend on the environment around the particles. For example, for our aqueous samples the dephasing time is solely determined by the distribution of sizes.[59,70] In contrast, from their studies of Ag particles in a glass, Del Fatti and co-workers concluded that the dephasing time has an important contribution from coupling to the environment, and that this coupling depends on the particle size.[60] On the other hand, the measured frequencies were very close to the values expected for a "free" particle, which means that embedding the particles in a glass does not affect the eigenvalues for the breathing mode.[60] To further investigate these effects, we have begun a series of experiments with core−shell nanoparticles. Using colloidal and radiation chemistry techniques particles of Au, Pt or Ag can be coated with silica,[73] or with other metals—such as Au,[27,28] Pb,[29] Pt[30] or Hg.[31] The thickness of the coating can be controlled, which provides flexibility for manipulating the environment around the particles. Our initial experiments were to compare the modulations for ~15 nm diameter Au particles with and without a silica shell. Both the frequency and the damping times were identical for these two samples. This is not surprising, as the silica shells around colloidal particles are porous and well hydrated.[74] Much more dramatic effect can be obtained with bimetallic particles.

Figure 10a shows transient absorption data for 47 nm diameter Au particles coated with Pb layers of different thickness.[62] These particles were formed by γ-irradiating a Au colloid-Pb$(ClO_4)_2$ solution until all the Pb^{2+} ions were reduced.[29] The number of atomic layers of Pb given in the figure was calculated from the particle diameter and the total concentrations of Au and Pb. The fast initial bleach signal is due to the hot electron gas created by the pump laser. As discussed above, the electrons relax by coupling to the phonon modes, and this occurs on a time scale of 2 to 5 ps at the pump laser powers used in these experiments (~0.05 mJ/pulse).[19] The remaining oscillatory signal at longer times arises from periodic modulation of the electron density in the particles, due to the coherently excited breathing motion.[62] Figure 10b shows a plot of the frequencies obtained by fitting the data to a damped cosine function. These results clearly show that the oscillation frequency decreases as the diameter increases (increasing Pb content). Note that the damping only slightly increases with increasing Pb, which indicates that the coated particles are reasonably monodisperse.

The reduction in frequency with increasing Pb content is expected for two reasons. First, the overall size of the particles has increased. Second, the deposited Pb layer has a lower speed of sound than the Au core: $c_l = 2160$ ms^{-1} for Pb compared to 3240 ms^{-1} for Au.[71] However, the decrease in frequency is smaller than that expected from the change in the particle size. For example, adding 20 Pb layers increases the radius by 25%, but only causes a 10% decrease in the breathing mode frequency. Allowing for the lower speed of sound of Pb in the calculation

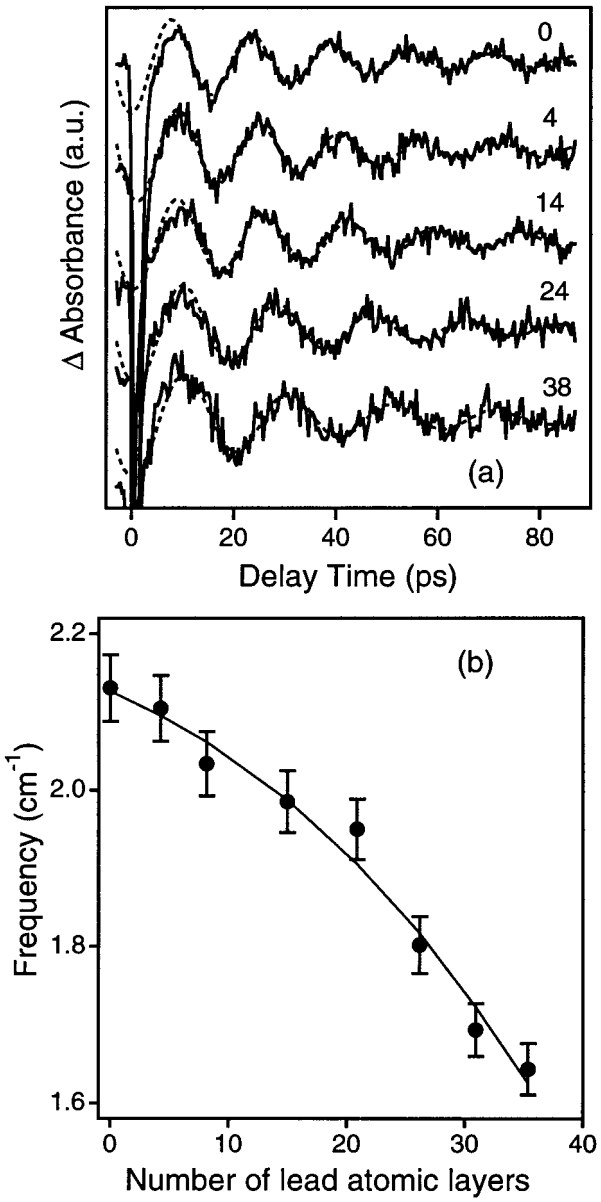

Figure 10. (a) Transient absorption data for 47 nm diameter Au particles coated with Pb layers of different thickness. (b) Breathing mode frequency versus Pb thickness. The solid line is a guide to the eye.

of η and $\bar{\nu}_R$ makes the agreement between the measured and calculated frequencies even worse! A physical interpretation of these results is that for small Pb layer thickness, the Pb layer "rides" on the motion of the core, and slightly lowers the resonant frequency of the particle. As the amount of Pb increases there is significant expansion/compression in both the core and the shell, producing a stronger decrease in the breathing mode frequency.[62,75] Obviously this is a very qualitative discussion. An accurate description of the acoustic breathing modes of core−shell nanoparticles requires that the equations of motion for the particles be solved with the correct boundary conditions, i.e., the difference in the elastic properties of the core and the shell must be explicitly taken into account.

Electron−Phonon Coupling in Bimetallic Particles. Measurements of e−ph coupling in Au films have shown that polycrystalline films have faster relaxation times compared to single-crystal films.[53] This is attributed to enhanced coupling between the electrons and phonons at the grain boundaries in the film. Metal particles that are synthesized by wet chemistry

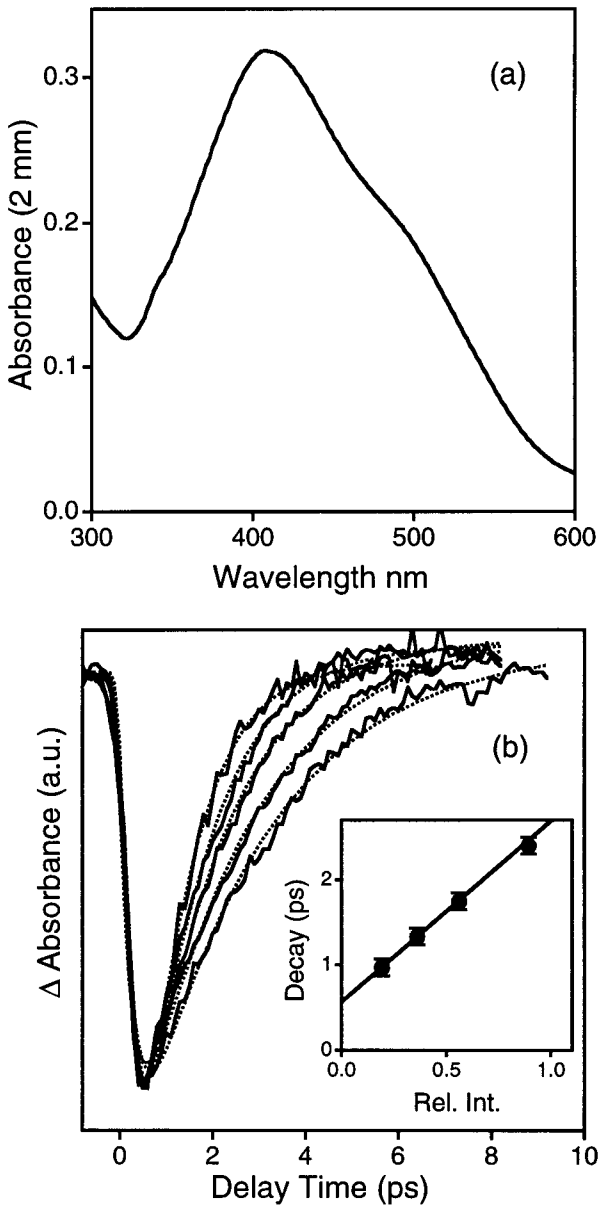

Figure 11. (a) Absorption spectrum of $Au_{core}Ag_{shell}$ particles prepared from 20 nm diameter Au cores with a 1:1 molar ratio of Au:Ag. (b) Transient absorption data obtained for the same sample with 410 nm pump and probe pulses. The inset shows a plot of the measured lifetime versus relative pump laser power.

techniques have a large number of defects, and whether these play a role in e−ph coupling is a significant question.[14] One way of testing how the presence of a boundary affects the coupling between the electrons and phonons is to engineer bimetallic particles with a well-defined interface between the metals. For example, Figure 2 shows a TEM micrograph of $Au_{core}Ag_{shell}$ nanoparticles where the interface between the Au and Ag can be clearly seen. Ag and Au have very similar e−ph coupling times.[14,18,19] Thus, if the boundary is important in mediating energy transfer between the electrons and the phonons, then these particles should show faster e−ph coupling times compared to pure Ag or Au particles.

An absorption spectrum of $Au_{core}Ag_{shell}$ particles with a molar ratio of Au:Ag = 1:1 is presented in Figure 11a. The spectrum displays two plasmon bands at ca. 500 and 410 nm that correlate with the plasmon bands for pure Au or Ag particles, respectively. (The 500 nm band appears as a shoulder on the stronger 410 nm band for these particles). Figure 11b shows time-resolved

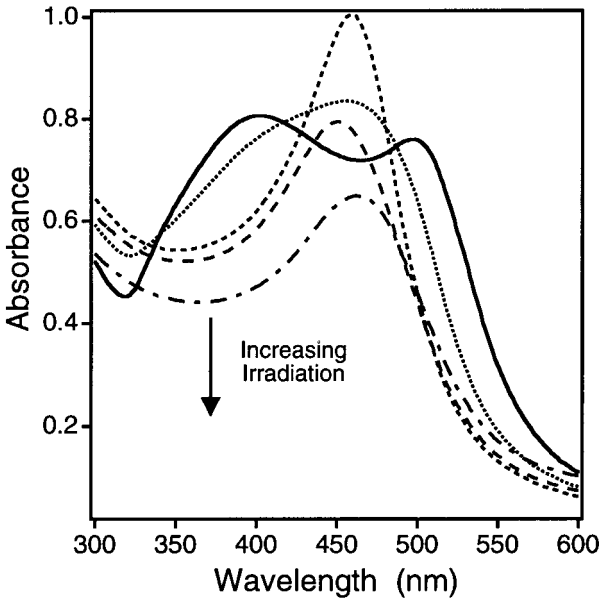

Figure 12. Absorption spectra (1 cm path length) of $Au_{core}Ag_{shell}$ particles prepared from 20 nm diameter cores with a 2:1 Au:Ag ratio before and after irradiation with 532 nm 30 ps laser pulses. The different curves correspond to absorbed energies of 0, 0.1, 1.2, 4.6, and 6.7 mJ $pulse^{-1}$.

data obtained with 410 nm pump and probe laser pulses. A plot of the measured time constants versus relative pump laser power is presented in the inset. As was observed for the Au particles, the decay times increase with pump laser power. The characteristic e−ph coupling time obtained from the data in Figure 11b is identical to that for pure Au or Ag particles.[18,19] Thus, the interface between the two metals does not contribute to the e−ph coupling.

The $Au_{core}Ag_{shell}$ particles provide an interesting system for examining laser-induced melting of metal particles. Nanosecond or picosecond laser pulses with mJ energies per pulse supply enough heat to melt metal particles. Previous experiments have examined the thermal reshaping of facetted Au particles (as produced by standard chemical reduction methods) into smooth spheres,[76] the fragmentation of ca. 60 nm diameter Ag particles,[77] and the transformation of Au nano-rods into spheres.[78,79] The growth of thiol derivatized Au particles following photoexcitation by 532 or 1064 nm laser pulses has also been reported.[80,81]

The driving force for the rod-to-sphere transition is that a spherical shape minimizes the surface energy. Au and Ag form an ideal solid mixture at all compositions.[82] Thus, laser-induced melting of $Au_{core}Ag_{shell}$ particles should produce alloys, the driving force being the entropy of mixing. The optical spectra of core−shell metal particles are significantly different to those for alloyed particles: core−shell particles typically display two plasmon bands,[28,37,38] whereas, alloyed particles have a single plasmon band located between those of the pure metal particles.[83] Thus, the core−shell to alloy transformation can be followed by recording UV−vis spectra after laser irradiation. This is shown in Figure 12 for $Au_{core}Ag_{shell}$ particles with an overall composition of Au:Ag = 1:0.5. The samples were irradiated by 532 nm 30 ps laser pulses for 15 min at 10 Hz repetition rate. Absorbed energies > 1 mJ $pulse^{-1}$ clearly transform the core−shell particles (two plasmon bands) into alloyed particles (single plasmon band at 460 nm). Higher energy pulses cause further spectral changes that are attributed to fragmentation—this has been confirmed by TEM analysis.[84]

There are several interesting points to note about these experiments. First, the energies per pulse needed to transform the particles are almost an order of magnitude lower for picosecond laser pulses compared to nanosecond laser pulses.[84] This is because there is significant heat transfer to the surrounding medium during the excitation for a nanosecond pulse. (Typical time scales for energy transfer from the particles to the solvent are 100−200 ps.) Second, laser-induced alloying does not occur in a single laser pulse, even at high powers. The particles do not remain molten long enough after excitation for the two metals to inter-diffuse. Many melting-diffusion-freezing steps must occur in order for the core−shell particles to become homogeneously alloyed.[84]

Summary and Conclusions

In many respects the physical properties of nanometer sized metal particles are identical to those of the bulk metal. For example, by using transient absorption spectroscopy we have been able to show that the characteristic time scale for energy exchange between the electrons and phonons for Au does not depend on size, for particles as small as 2.5 nm diameter.[19] This conclusion agrees with that of El-Sayed and co-workers,[14] and simply reflects that the coupling to the surface phonon modes for these particles is much weaker than the bulk electron−phonon coupling. Time-resolved spectroscopy also provides information about the elastic properties of the particles. Specifically, the rapid heating that accompanies ultrafast laser excitation impulsively excites the symmetric breathing mode of the particles, which produces a beat signal in our transient absorption experiments.[22,59,62] The measured frequencies exactly match the predictions of classical mechanics calculations for Au particles larger than ca. 8 nm. These calculations involve both the transverse and longitudinal speeds of sound, thus, the elastic modulii that determine the speeds of sound are independent of size for Au. For particles smaller than 8 nm the period of the breathing motion is similar to the time scale for lattice heating, so that impulsive excitation of the breathing mode is no longer possible.

Our recent work has centered on bimetallic core−shell nanoparticles. These unique materials are synthesized using radiation chemistry techniques. Shells of different metals and thickness can be grown around seed particles by varying the type and concentration of the metal ions in solution. Both the acoustic breathing modes and the coupling between the electrons and phonons are of interest for these materials. Initial experiments with $Au_{core}Pb_{shell}$ particles show that the frequency of the breathing mode decreases with increasing thickness of the Pb shell, but not to the extent expected from the increase in the size of the particles. These experiments show that the difference in elastic properties of the core and the shell must be explicitly taken into account in order to understand the acoustic modes of these particles. On the other hand, experiments with $Au_{core}Ag_{shell}$ particles demonstrate that the interface does not enhance the coupling between the electrons and phonons. The core−shell particles can be transformed into alloyed particles by laser-induced melting. Homogeneous alloying requires many laser pulses, because inter-diffusion is much slower than heat dissipation for nanometer sized particles. The combination of radiation chemistry and laser-induced melting provides an intriguing way of synthesizing metal particles with unique—and controllable—properties.

Acknowledgment. The work described here was supported by the NSF, Grant No. CHE98-16164 (G.V.H. and J.H.H.) and by the U.S. Department of Energy, Office of Basic Energy Sciences (A.H.). We are deeply indebted to Michael Giersig of the Hahn-Meitner Institute (Berlin) for the electron micrograph measurements. This is document NDRL No. 4232 from the Notre Dame Radiation Laboratory. J.H.H. is thankful for the Peter Grace Fellowship administered by the University of Notre Dame.

References and Notes

(1) Buffat, P.; Borel, J.-P. *Phys. Rev. A* **1976**, *13*, 2287.
(2) Allen, G. L.; Bayles, R. A.; Giles, W. W.; Jesser, W. A. *Thin Solid Films* **1986**, *144*, 297.
(3) (a) Goldstein, A. N.; Echer, C. M.; Alivisatos, A. P. *Science* **l992**, *256*, l425. (b) Tolbert, S. H.; Alivisatos, A. P. *Annu. Rev. Phys. Chem.* **1995**, *46*, 595.
(4) Bawendi, M. G.; Steigerwald, M. L.; Brus, L. E. *Annu. Rev. Phys. Chem.* **1990**, *41*, 477.
(5) de Heer, W. A. *Rev. Mod. Phys.* **1993**, *65*, 611.
(6) Alivisatos, A. P. *J. Phys. Chem.* **1996**, *100*, 13226.
(7) Andres, R. P.; Bein, T.; Dorogi, M.; Feng, S.; Henderson, J. I.; Kubiak, C. P.; Mahoney, W.; Osifchin, R. G.; Reifenberger, R. *Science* **1996**, *272*, 1323.
(8) Klein, D. L.; Roth, R.; Lim, A. K. L.; Alivisatos, A. P.; McEuen, P. L. *Nature* **1997**, *389*, 699.
(9) Chen, S. W.; Ingram, R. S.; Hostetler, M. J.; Pietron, J. J.; Murray, R. W.; Schaaff, T. G.; Khoury, J. T.; Alvarez, M. M.; Whetten, R. L. *Science* **1998**, *280*, 2098.
(10) Kim, S. H.; Medeiros-Ribeiro, G.; Ohlberg, D. A. A.; Williams, R. S.; Heath, J. R. *J. Phys. Chem. B* **1999**, *103*, 10341.
(11) Valden, M.; Lai, X.; Goodman, D. W. *Science* **1998**, *281*, 1647.
(12) (a) Roberti, T. W.; Smith, B. A.; Zhang, J. Z. *J. Chem. Phys.* **1995**, *102*, 3860. (b) Smith, A.; Zhang, J. Z.; Griebel, U.; Schmid, G. *Chem. Phys. Lett.* **1997**, *270*, 139. (c) Zhang, J. Z. *Acc. Chem. Res.* **1997**, *30*, 423.
(13) (a) Bigot, J. Y.; Merle, J. C.; Cregut, O.; Daunois, A. *Phys. Rev. Lett.* **1995**, *75*, 4702. (b) Shabazyan, T. V.; Perakis, I. E.; Bigot, J. Y. *Phys. Rev. Lett.* **1998**, *81*, 3120. (c) Bigot, J. Y.; Halte, V.; Merle, J. C.; Daunois, A. *Chem. Phys.* **2000**, *251*, 181.
(14) (a) Ahmadi, T. S.; Logunov, S. L.; El-Sayed, M. A. *J. Phys. Chem.* **1996**, *100*, 8053. (b) Logunov, S. L.; Ahmadi, T. S.; El-Sayed, M. A.; Khoury, J. T.; Whetten, R. L. *J. Phys. Chem. B* **1997**, *101*, 3713. (c) Link, S.; Burda, C.; Wang, Z. L.; El-Sayed, M. A. *J. Chem. Phys.* **1999**, *111*, 1255. (d) Link, S.; El-Sayed, M. A. *J. Phys. Chem. B* **1999**, *103*, 8410.
(15) (a) Stella, A.; Nisoli, M.; De Silvestri, S.; Svelto, O.; Lanzani, G.; Cheyssac, P.; Kofman, R. *Phys. Rev. B* **1996**, *53*, 15497. (b) Nisoli, M.; Stagira, S.; De Silvestri, S.; Stella, A.; Tognini, P.; Cheyssac, P.; Kofman, R. *Phys. Rev. Lett.* **1997**, *78*, 3575. (c) Stagira, S.; Nisoli, M.; De Silvestri, S.; Stella, A.; Tognini, P.; Cheyssac, P.; Kofman, R. *Chem. Phys.* **2000**, *251*, 259.
(16) Feldstein, M. J.; Keating, C. D.; Liau, Y. H.; Natan, M. J.; Scherer, N. F. *J. Am. Chem. Soc.* **1997**, *119*, 6638.
(17) Perner, M.; Bost, P.; Lemmer, U.; von Plessen, G.; Feldmann, J.; Becker, U.; Mennig, M.; Schmitt, M.; Schmidt, H. *Phys. Rev. Lett.* **1997**, *78*, 2192.
(18) (a) Del Fatti, N.; Flytzanis, C.; Vallée, F. *App. Phys. B* **1999**, *68*, 433. (b) Hamanaka, Y.; Nakamura, A.; Omi, S.; Del Fatti, N.; Vallée, F.; Flytzanis, C. *App. Phys. Lett.* **1999**, *75*, 1712. (c) Del Fatti, N.; Vallée, F.; Flytzanis, C.; Hamanaka, Y.; Nakamura, A. *Chem. Phys.* **2000**, *251*, 215.
(19) (a) Hodak, J. H.; Martini, I.; Hartland, G. V. *Chem. Phys. Lett.* **1998**, *284*, 135. (b) Hodak, J. H.; Martini, I.; Hartland, G. V. *J. Phys. Chem. B* **1998**, *102*, 6958. (c) Hodak, J. H.; Henglein, A.; Hartland, G. V. *J. Chem. Phys.* **2000**, *112*, 5942.
(20) (a) Averitt, R. D.; Westcott, S. L.; Halas, N. J. *Phys. Rev. B* **1998**, *58*, R10203. (b) Averitt, R. D.; Westcott, S. L.; Halas, N. J. *J. Opt. Soc. Am. B* **1999**, *16*, 1814.
(21) Inouye, H.; Tanaka, K.; Tanahashi, I.; Hirao, K. *Phys. Rev. B* **1998**, *57*, 11334.
(22) Hodak, J. H.; Martini, I.; Hartland, G. V. *J. Chem. Phys.* **1998**, *108*, 9210.
(23) Zewail, A. H. *Femtochemistry: Ultrafast Dynamics of the Chemical Bond*, World Scientific: Singapore, 1994.
(24) El-Sayed, M. A.; Tanaka, I.; Molin, Y. *Ultrafast Processes in Chemistry and Photobiology*, Blackwell Science: Cambridge, 1995.
(25) Mukamel, S. *Principles of Nonlinear Optical Spectroscopy*; Oxford University Press: New York, 1995.
(26) Henglein, A. *J. Phys. Chem.* **1993**, *97*, 5457.
(27) (a) Henglein, A.; Meisel, D. *Langmuir* **1998**, *14*, 7392. (b) Henglein, A. *Langmuir* **1999**, *15*, 6738.
(28) Mulvaney, P.; Giersig, M.; Henglein, A. *J. Phys. Chem.* **1993**, *97*, 7061.

(29) Mulvaney, P.; Giersig, M.; Henglein, A. *J. Phys. Chem.* **1992**, *96*, 10419.
(30) Henglein, A. *J. Phys. Chem. B* **2000**, *104*, 2201.
(31) Henglein, A.; Giersig, M. *J. Phys. Chem. B* **2000**, *104*, 5056.
(32) Henglein, A.; Lilie, J. *J. Am. Chem. Soc.* **1981**, *103*, 1059.
(33) Enüstün, B. V.; Turkevich, J. *J. Am. Chem. Soc.* **1963**, *85*, 3317.
(34) (a) Ahmadi, T. S.; Wang, Z. L.; Green, T. C.; Henglein, A.; El-Sayed, M. A. *Science* **1996**, *272*, 1924. (b) Henglein, A.; Giersig M. *J. Phys. Chem. B* **2000**, *104*, 6767.
(35) Van de Hulst, H. C. *Light Scattering by Small Particles*; Dover: New York, 1981.
(36) Bohren, C. F.; Huffman, D. R. *Absorption and Scattering of Light by Small Particles*; Wiley: New York, 1983.
(37) Kreibig, U.; Vollmer, M. *Optical Properties of Metal Clusters*; Springer: Berlin, 1995.
(38) Mulvaney, P. *Langmuir* **1996**, *12*, 788.
(39) (a) Rosei, R.; Lynch, D. W *Phys. Rev. B* **1972**, *5*, 3883. (b) Rosei, R.; Antonangeli, F.; Grassano, U. M. *Surf. Sci.* **1973**, *37*, 689.
(40) (a) Ehrenreich, H.; Philipp, H. R. *Phys. Rev.* **1962**, *128*, 1622. (b) Johnson, P. B.; Christy, R. W. *Phys. Rev. B* **1972**, *6*, 4370.
(41) Ashcroft, N. W.; Mermin, N. D. *Solid State Physics*; Harcourt Brace: Orlando, FL, 1976.
(42) Doremus, R. H. *J. Chem. Phys.* **1965**, *42*, 414.
(43) Kraus, W. A.; Schatz, G. C. *J. Chem. Phys.* **1983**, *79*, 6130.
(44) Kreibig, U.; Genzel, U. *Surf. Sci.* **1985**, *156*, 678.
(45) (a) Doremus, R. H.; Rao, P. *J. Mater. Res.* **1996**, *11*, 2834. (b) Doremus, R. H. *Thin Solid Films* **1998**, *326*, 205.
(46) (a) Alvarez, M. M.; Khoury, J. T.; Schaaff, T. G.; Shafigullin, M. N.; Vezmar, I.; Whetten, R. L. *J. Phys. Chem. B* **1997**, *101*, 3706. (b) Schaaff, T. G.; Shafigullin, M. N.; Khoury, J. T.; Vezmar, I.; Whetten, R. L.; Cullen, W. G.; First, P. N.; Gutierrez Wing, C.; Ascensio, J.; Jose Yacaman, M. J. *J. Phys. Chem. B* **1997**, *101*, 7885.
(47) Klar, T.; Perner, M.; Grosse, S.; von Plessen, G.; Spirkl, W.; Feldmann, J. *Phys. Rev. Lett.* **1998**, *80*, 4249.
(48) (a) Fann, W. S.; Storz, R.; Tom, H. W. K.; Bokor, J. *Phys. Rev. B* **1992**, *46*, 13592. (b) Fann, W. S.; Storz, R.; Tom, H. W. K.; Bokor, J. *Phys. Rev.* Lett. **1992**, *68*, 2834.
(49) Schmuttenmaer, C. A.; Aeschlimann, M.; Elsayed-Ali, H. E.; Miller, R. J. D.; Mantell, D. A.; Cao, J.; Gao, Y. *Phys. Rev. B* **1994**, *50*, 8957.
(50) Hertel, T.; Knoesel, E.; Wolf, M.; Ertl, G. *Phys. Rev. Lett.* **1996**, *76*, 535.
(51) Ogawa, S.; Nagano, H.; Petek, H. *Phys. Rev. B* **1997**, *55*, 10869.
(52) Knorren, R.; Bennemann, K. H.; Burgermeister, R.; Aeschlimann, M. *Phys. Rev. B* **2000**, *61*, 9427.
(53) (a) Elsayed-Ali, H. E.; Norris, T. B.; Pessot, M. A.; Mourou, G. A. *Phys. Rev. Lett.* **1987**, *58*, 1212. (b) Elsayed-Ali, H. E.; Juhasz, T.; Smith, G. O.; Bron, W. E. *Phys. Rev. B* **1991**, *43*, 4488.
(54) (a) Schoenlein, R. W.; Lin, W. Z.; Fujimoto, J. G.; Eesley, G. L. *Phys. Rev. Lett.* **1987**, *58*, 1680. (b) Brorson, S. D.; Fujimoto, J. G.; Ippen, E. P. *Phys. Rev. Lett.* **1987**, *59*, 1962.
(55) (a) Groeneveld, R. H. M.; Sprik, R.; Lagendijk, A. *Phys. Rev. Lett.* **1990**, *64*, 784. (b) Groeneveld, R. H. M.; Sprik, R.; Lagendijk, A. *Phys. Rev. B* **1995**, *51*, 11433.
(56) (a) Sun, C.-K.; Vallée, F.; Acioli, L. H.; Ippen, E. P.; Fujimoto, J. G. *Phys. Rev. B* **1993**, *48*, 12365. (b) Sun, C.-K.; Vallée, F.; Acioli, L. H.; Ippen, E. P.; Fujimoto, J. G. *Phys. Rev. B* **1994**, *50*, 15337.
(57) (a) Belotskii, E. D.; Tomchuk, P. M. *Surf. Sci.* **1990**, *239*, 143. (b) Belotskii, E. D.; Tomchuck, P. M. *Int. J. Electron.* **1992**, *73*, 955.
(58) Nisoli, M.; De Silvestri, S.; Cavalleri, A.; Malvezzi, A. M.; Stella, A.; Lanzani, G.; Cheyssac, P.; Kofman, R. *Phys. Rev. B* **1997**, *55*, R13424.
(59) Hodak, J. H.; Henglein, A.; Hartland, G. V. *J. Chem. Phys.* **1999**, *111*, 8613.
(60) (a) Del Fatti, N.; Tzortzakis, S.; Voisin, C.; Flytzanis, C.; Vallée, F. *Physica B* **1999**, *263*, 54. (b) Del Fatti, N.; Voisin, C.; Chevy, F.; Vallée, F.; Flytzanis, C. *J. Chem. Phys.* **1999**, *110*, 11484. (c) Del Fatti, N.; Voisin, C.; Christofilos, C.; Vallée, F.; Flytzanis, C. *J. Phys. Chem. A* **2000**, *104*, 4321.
(61) Qian, W.; Lin, L.; Deng, Y. J.; Xia, Z. J.; Zou, Y. H.; Wong, G. K. L. *J. Appl. Phys.* **2000**, *87*, 612.
(62) Hodak, J. H.; Henglein, A.; Hartland, G. V. *J. Phys. Chem B* **2000**, *104*, 5053.
(63) Lamb, H. *Proc. London Math. Soc.* **1882**, *13*, 189.
(64) Dubrovskiy, V. A.; Morochnik, V. S. *Izv. Earth Phys.* **1981**, *17*, 494.
(65) Krauss, T. D.; Wise, F. W. *Phys. Rev. Lett.* **1997**, *79*, 5102.
(66) Thoen, E. R.; Steinmeyer, G.; Langlois, P.; Ippen, E. P.; Tudury, G. E.; Brito Cruz, C. H.; Barbosa, L. C.; Cesar, C. L. *Appl. Phys. Lett.* **1998**, *73*, 2149.
(67) (a) Cheng, T. K.; Vidal, J.; Zieger, H. J.; Dresselhaus, G.; Dresselhaus, M. S.; Ippen, E. P. *Appl. Phys. Lett.* **1991**, *59*, 1923. (b) Zieger, H. J.; Vidal, J.; Cheng, T. K.; Ippen, E. P.; Dresselhaus, G.; Dresselhaus, M. S. *Phys. Rev. B* **1992**, *45*, 768.
(68) (a) Duggal, A. R.; Rogers, J. A.; Nelson, K. A. *J. Appl. Phys.* **1992**, *72*, 2823. (b) Rogers, J. A.; Dhar, L.; Nelson, K. A. *Appl. Phys. Lett.* **1994**, *65*, 312. (c) Crimmins, T. F.; Maznev, A. A.; Nelson, K. A. *Appl. Phys. Lett.* **1999**, *74*, 1344.
(69) (a) Rogers, J. A.; Fuchs, M.; Banet, M. J.; Hanselman, J. B.; Logan, R.; Nelson, K. A. *Appl. Phys. Lett.* **1997**, *71*, 225. (b) Banet, M. J.; Fuchs, M.; Rogers, J. A.; Reinhold: J. H.; Knecht, J. M.; Rothschild, M.; Logan, R.; Maznev, A. A.; Nelson, K. A. *Appl. Phys. Lett.* **1998**, *73*, 169.
(70) Hodak, J. H.; Henglein, A.; Hartland, G. V. *Pure Appl. Chem.* **2000**, *72*, 189.
(71) *CRC Handbook of Chemistry and Physics*, 80th ed.; CRC Press: Boca Raton, FL, 1999.
(72) Shirahatti, U. S.; Crocker, M. J. In *Handbook of Acoustics*; Crocker, M. J., Ed.; John Wiley & Sons: New York, 1998; Chapter 6.
(73) (a) Liz-Marzan, L. M.; Giersig, M.; Mulvaney, P. *Chem. Commun.* **1996**, 731. (b) Liz-Marzan, L. M.; Giersig, M.; Mulvaney, P. *Langmuir* **1996**, *12*, 4329.
(74) (a) Giersig, M.; Ung, T.; Liz-Marzan, L. M.; Mulvaney, P. *Adv. Mater.* **1997**, *9*, 570. (b) Ung, T.; Liz-Marzan, L. M.; Mulvaney, P. *Langmuir* **1998**, *14*, 3740.
(75) Norton, M. P. *Fundamentals of Noise and Vibration Analysis for Engineers*; Cambridge University Press: Cambridge, MA, 1989.
(76) (a) Kurita, H.; Takami, A.; Koda, S. *App. Phys. Lett.* **1998**, *72*, 789. (b) Takami, A.; Kurita, H.; Koda, S. *J. Phys. Chem. B* **1999**, *103*, 1226.
(77) Kamat, P. V.; Flumiani, M.; Hartland, G. V. *J. Phys. Chem. B* **1998**, *102*, 3123.
(78) (a) Link, S.; Burda, C.; Mohamed, M. B.; Nikoobakht, B.; El-Sayed, M. A. *J. Phys. Chem. A* **1999**, *103*, 1165. (b) Link, S.; Burda, C.; Nikoobakht, B.; El-Sayed, M. A. *Chem. Phys. Lett.* **1999**, *315*, 12. (c) Link, S.; Burda, C.; Nikoobakht, B.; El-Sayed, M. A. *J. Phys. Chem. B* **2000**, *104*, 6152.
(79) Chang, S. S.; Shih, C. W.; Chen, C. D.; Lai, W. C.; Wang, C. R. C. *Langmuir* **1999**, *15*, 701.
(80) Fujiwara, H.; Yanagida, S.; Kamat, P. V. *J. Phys. Chem. B* **1999**, *103*, 2589.
(81) Niidome, Y.; Hori, A.; Sato, T.; Yamada, S. *Chem. Lett.* **2000**, 310.
(82) *Binary Alloy Phase Diagrams*; Massalski, T. B., Ed.; ASM International: Materials Park, OH, 1990.
(83) Link, S.; Wang, Z. L.; El-Sayed, M. A. *J. Phys. Chem. B* **1999**, *103*, 3529.
(84) Hodak, J. H.; Henglein, A.; Giersig, M.; Hartland, G. V. *J. Phys. Chem. B,* accepted for publication.